Photoinduced Doping of Nickel(II) ion in Nanoscale Zinc Oxide Semiconductor

S. Thirumurugan, A. S. Ganeshraja, K. Anbalagan*
Department of Chemistry, Pondicherry University, Pondicherry 605 014, India
e-mail: kanuniv@gmail.com, Tel: +91 413 2654509

Abstract: **- A sensitive doping of nickel(II) ion was achieved in nanosized ZnO lattice using excited ZnO and $Ni(py)_4Cl_2$ complex system. The latter was doused with λ = 254 nm light radiation in Pr^iOH / water medium for different time intervals. This generates active metal ion, which gets implanted into the lattice of ZnO. Pure and nickel implanted nanocrystalline ZnO were subjected to DRS, RAMAN, PL, LT, PXRD and BET surface area analysis to probe the characteristics of the surface. Life time studies were made on the Ni(II) implanted ZnO compound. The steady state emission spectra indicate shifts in the emission maxima from 825 → 822 nm. In addition, the band gap energy was found to be shifted from 3.22 to 3.18 eV as the dopant concentration is increased. Here, we focus on the understanding of the modification of ZnO surface by $Ni^{II}(py)_4Cl_2$ complex, which was attached by nitrogen linkers. Such modified surface:complex system is a precursor for the doping process. The experimental results yield the characteristic features on the inclusion of nickel(II) ion in ZnO.**

Keywords: Raman; Band gap energy; Nano-ZnO; BET

I. INTRODUCTION

The synthesis and functionalism of nanostructures have attracted great interest due to their significant potential application. Recently, semiconductor nanostructures have attracted much interest due to their extraordinary physical properties and potentials for diverse electronic and photonic device applications [1,2]. ZnO is one of the most promising materials for potential applications in spintronics and as diluted magnetic semiconductor (DMS) material. Among doped ZnO materials, 3d transition metals doped ZnO produces high quality DMS [3]. In this paper, Ni doped ZnO nanocrytalline film preparation and their characterizations are discussed. The researches on the synthesis and experimental characterizations of the nanostructures for diluted magnetic semiconductor (DMS) at room temperature have gained momentum. In order to fully understand these unique properties and explore the application of ZnO nanostructures on the design of high-performing nanodevices, great efforts are dedicated to rational synthesis of ZnO nanostructures and a rich family of ZnO nanostructures has been developed, including nanowires, nanosheets, nanotubes, nanobelts and nanorings, *etc* [4-6].

II. EXPERIMENTAL

2.1. Materials and methods

Nano-crystalline Zinc(II) oxide was purchased from Sigma Aldrich. Nickel(II) chloride hexahydrate, Sodium perchlorate and pyridine were purchased from Himedia (India). All the solvents were purified by distillation and water was triply distilled over alkaline $KMnO_4$ in all glass apparatus. The Ni(II)/nano-ZnO sample was analyzed by diffuse reflectance spectroscopy, Raman spectroscopy, photoluminescence spectroscopy, life time measurements, powder X-Ray diffraction, surface area (BET) analyzer.

2.2. Photocatalyst procedure

Photoreduction was carried out in a reactor vessel using 254 nm low pressure mercury vapor lamp, which were housed in a fume hood (Lab Guard), covered with black polythene sheet to prevent extraneous light. The photoreactor is double walled quartz vessel, in which, photolyte mixture (200 mg of nano-ZnO crystals in 80 mL of $Ni^{II}(py)_4Cl_2$ (4.2×10^{-4}M) solution and 0.05 M $NaClO_4$) was taken in the inner jacket and cool water in the outer jacket. Prior to irradiation, the suspension of the catalyst was achieved by ultrasonic treatment and continued to stir magnetically in dark to attain nickel(II) complex ion adsorption/desorption equilibrium on the catalyst. The photolytic suspension was doused with 254 nm light for definite irradiation periods (0, 2, 4, 8, 12, 16 min). About 4 mL aliquots were sampled and centrifuged to remove the semiconductor particles and then spectrally analysed. In order to diminish the experimental error, the experiments were repeated at least two-three times for the same sample and calculated the mean value.

III. RESULTS AND DISCUSSION

Photochemical reduction of $Ni^{II}(py)_4Cl_2$ complex was followed in presence of nano-ZnO in water/2-propanol solvent mixture at 254 nm light. Nickel(II)-pyridine complex is a good UV light absorber, however, decomposes on exposure to light over a long period of time due to ligand to metal charge transfer (LMCT) band at 365 nm as shown in Figure 1. The LMCT band (λ = 365 nm) increases due to UV irradiation. Repetitive scan spectral study confirms that Ni(II)-pyridine complex is readily photoreduced in presence of nano-ZnO.

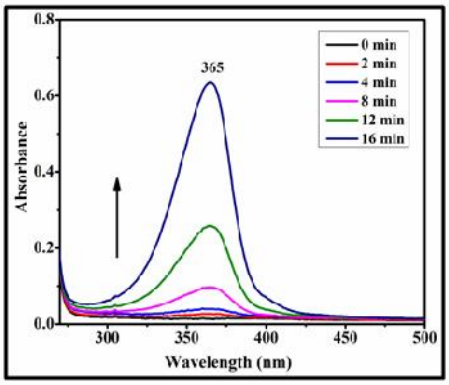

FIGURE 1 Repetitive scan spectra recorded for the photocatalysed reduction of $Ni^{II}(py)_4Cl_2$ /nano-ZnO in 30/70 (w/w)% Pr^iOH/water at various time intervals. Irradiation wavelength λ = 254 nm. Medium: 0.05 M $NaClO_4$ and at 300 k.

3.1. Diffuse Reflectance Spectra

Diffuse reflectance spectra were recorded to estimate the optical band gap of the pure and nickel doped zinc oxide (Fig. 2(a)). Fig. 2(b) shows a plot for the percentage of reflection as a function of band gap energy (hυ) of the nanoparticles obtained from photoreaction. The doped ZnO samples exhibit absorption peaks in the visible region in addition to the absorption edge, due to bands from crystal-field transitions of Ni(II) ions in tetrahedral coordination. As an example, the absorption spectrum of Ni(II) doped ZnO shows the mid-band-gap states appearing at about 416-425 nm as band edge, with corresponding d-d transition bands at ~665 nm, which is characteristic of Ni(II) with tetrahedral symmetry. In the case of Ni doped ZnO, absorption peaks are expected to arise due to electronic transitions from the $^3T_1(F)$ ground state to the $^3T_1(P)$ state for the tetrahedral Ni(II) species [7]. As seen in the Fig. 2(a), an absorption peak of the Ni doped ZnO is shifted from 665 to 659nm, which is strongly blue shifted from undoped ZnO (Table 1). The blue shifted absorption of all the doped samples reveals the decrease of the band gap energy from 3.22 to 3.18 eV (Table 1). This may be due to quantum confinement effect.

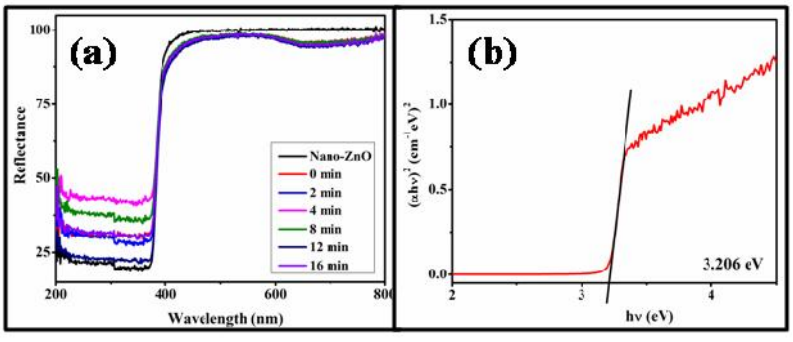

FIGURE 2 (a) DRS spectrum and (b) Band gab energy graph of sample collected from photolysis reaction of $Ni^{II}(py)_4Cl_2$ complex with nano-ZnO in 30/70 (w/w)% Pr^iOH/water at various time intervals: respectively. Irradiation wavelength λ = 254 nm. Medium: 0.05M $NaClO_4$ and at 300 k.

TABLE 1 Band gap energy values, PXRD data and Specific surface area for Ni/nano-ZnO obtained from photocatalysed reaction of NiII(py)4Cl2 complex with nano-ZnO in 30/70 (w/w)% PriOH/water at various time intervals: Irradiation wavelength λ = 254 nm. Medium: 0.05M NaClO4 and at 300 k.

Irradiation time (min)	direct band gap energy (eV)	absorption edge (nm)	λ_{max} (nm)	PXRD data			BET analysis
				2θ	Intensity (a.u.)	Particle size (nm)	Surface Area (m^2/g)
Nano-ZnO	3.22	416.1	-	--	--	70.5	15.748
0	3.21	424.0	665	47.6	290	82.4	12.485
2	3.19	425.0	661	47.6	303	90.4	12.838
4	3.18	424.5	663	Not measured			12.643
8	3.20	422.7	665	47.5	315	86.0	12.729
12	3.22	425.2	659	Not measured			12.954
16	3.21	423.7	660	47.5	368	93.5	13.525

3.2. **Powder X-ray diffraction analysis**

The powder X-ray diffraction patterns of the undoped and Ni doped ZnO are shown in Fig. 3. It is evident that the C-axis orientation peak is prominent over the other peaks than that of pure ZnO hexagonal structure. No additional peaks are observed due to any of impurity. The sharp and intense peaks indicate that the samples are highly crystalline nature. The XRD peaks for (100), (002), (101), (102), (110), (103) and (112) planes indicates the formation of phase pure wurtzite structure of ZnO. The crystallite size of Ni-doped ZnO is calculated using Scherrer's formula [8-12] and given in Table 1. It is seen from Fig. 3, that all the samples dominant in peaks such as (100), (002) and (101). The average particle size of doped ZnO, that is obtained at 16 min irradiation period (25 nm) is increased than pure ZnO. However, the intensities of diffraction peaks decline as the Ni^{2+} ion concentration increases, the nickel doping within the particle causes the ZnO crystallinity to deteriorate. The intensity of diffraction peaks becomes weaker and the half-peak width becomes wider as the dopant concentration, Ni^{2+} ions inhibit the process of crystallization of ZnO nanocrystals [**9].**

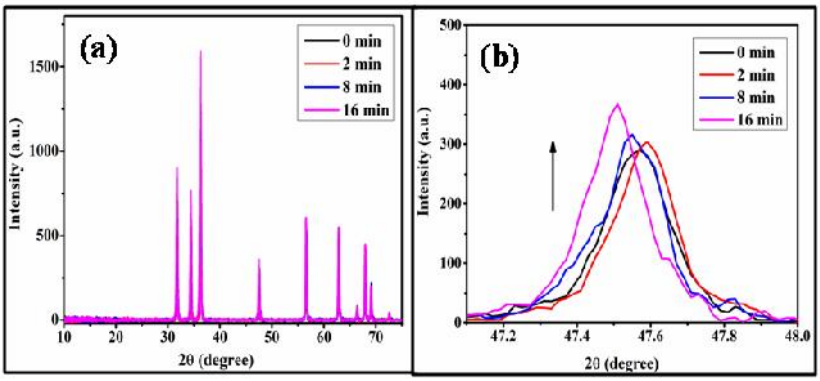

FIGURE 3 PXRD pattern of Ni(II):nano-ZnO particles isolated from photosolution of $Ni^{II}(py)_4Cl_2$ complex with nano-ZnO.

3.3. Raman Spectral and BET Surface Area Analysis of Ni:nano-ZnO

Fig. 4(a) shows room temperature Raman spectra over a range from 0 to 2000 cm^{-1}. The assignments of the Raman peaks of the ZnO nanoparticles are labelled in the Figure in accordance with reported Raman studies on ZnO [13]. The high frequency branch of E_{2H} mode involves the oxygen motion as well as sensitive to internal stress is characteristic of good wurtzite structure of ZnO nano size,[14–17] that mode has a drastic reduction in intensity once doped. It is found that the Raman spectra of sample shows no extra peaks due to impurity or host lattice defects. So it can be regarded that the nanoparticles obtained in this experiment are pure and crystallized well [14].

The surface area data given in Table 1 demonstrate that doping of metal on ZnO particles does induce appreciable change in the surface area. It is observed that surface area decreased, 13.525 m^2/g for Ni/nano-ZnO

when compared with pure nano-ZnO (15.748 m^2/g). Hence the decrease in surface area of Ni-loaded ZnO might be due to blocking of fine capillaries of parent ZnO surface [18].

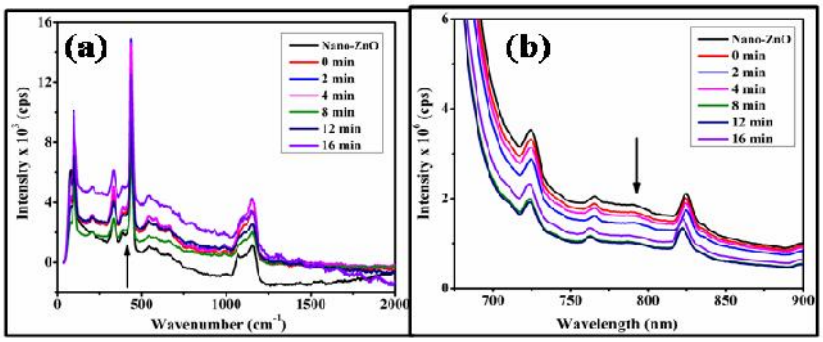

FIGURE 4 (a) Raman spectrum and (b) Steady state emission spectrum of sample collected from photolysis reaction of $Ni^{II}(py)_4Cl_2$complex with nano-ZnO in 30/70 (w/w)% Pr^iOH/water at various time intervals. Irradiation wavelength λ = 254 n m. Medium: 0.05M $NaClO_4$ and at 300 k.

3.4. Photophysical measurements of Ni:ZnO

Fig. 4(b) shows the room temperature photoluminescence spectra of pristine and co-doped (Ni) ZnO nanostructures with six different doping concentrations. The PL spectrum exhibits three emission bands in visible region, under high excitation energy ~ 3.65eV. In the UV spectral range from 660 to 665 nm, the intense narrow emission band has appeared in the range 725 to 825 nm. In general, the UV emission band is the characteristic emission of ZnO and it is attributed to the free excitonic recombination or zinc vacancy related defects in ZnO [9-10,19].

TABLE 2 Life times measured for nano-ZnO isolated from photocatalysed reaction of $[Ni^{II}(py)_4Cl_2]$ complex with nano-ZnO in 30/70 (w/w)% Pr^iOH/water at various time intervals. Irradiation wavelength λ = 254 nm. Medium: 0.05M $NaClO_4$. intensity, 1 x 10^{18} Einstein s^{-1}, LMCT band at368 nm and monitoring at 50 – 1000 ns, Nano-LED 295 nm and at 300 k.

S. No.	Irradiation time (min)	Emission data λ_{emi} (nm)			Excited state life time parameters τ_1, ns	τ_2, ns	τ_3, ns	χ^2
1.	Nano-ZnO	724.5	764.9	824.5	0.11	0.35	3.12	1.00
2.	0	724.5	764.4	824.4	0.47	0.15	3.05	0.87
3.	2	724.3	764.8	824.6	0.54	3.61	0.09	1.06
4.	4	724.3	764.9	824.3	0.12	0.47	3.41	0.94
5.	8	723.7	762.6	822.0	0.18	1.21	3.78	0.95
6.	12	723.7	762.4	821.9	0.18	1.62	6.00	0.89
7.	16	723.7	762.6	821.9	0.16	0.36	2.51	1.07

On increasing the nickel doping concentration in ZnO, there is a small change (i.e. slightly shifted towards lower wave length side) in position of the UV emission band. This is presumed to be due to a decrease of the size of ZnO nanoparticle. The PL intensity is low for co-doped ZnO nanoparticles as compared to those of undoped ZnO [9]. But, the doped ZnO has another defect related broad emission peak in the visible region around 725 to 825 nm, which is associated with Zn interstitial defect states. Therefore, emissions likely originate from surface defects, such as ionizable oxygen vacancies or zinc vacancies. The photoluminescence result is that the dopant induces geometrical distortions (contractions) of the neighboring oxygen vacancy, and hence the emission intensity is altered. Excited state life time data for Ni/ZnO as presented in Table 2 showed triexponential kinetics.

II. CONCLUSION

In summary, nanocrystalline Ni-doped ZnO were successfully synthesized by photochemical method. XRD analysis reveals the formation of hexagonal wurtzite structure of nickel doped ZnO samples obtained from irradiation. XRD patterns and Raman spectra proved the incorporation nickel into the ZnO lattice. PL confirmed implantation of Ni(II) doped ZnO and DRS analysis yielded the band gap energy values. The structure and phase purity of the samples were determined using X-ray diffraction method. The size of the particles were determined using Debye Scherer's formula.

ACKNOWLEDGMENT

KA is thankful to the CSIR (sanction order: No. 01(2570)/12/EMR-II/3.4.2012), New Delhi for financial support through major research project. The authors are thankful to CIF, Pondicherry University for instrumental facility.

REFERENCES

[1] X. Duan, Y. Huang, Y. Cui, J. Wang and C. M. Lieber "Indium phosphide nanowires as building blocks for nanoscale electronic and optoelectronic devices," Nature, vol. 409, pp. 66-69, January 2001.

[2] Z. L. Wang, "Zinc oxide nanostructures: growth, properties and applications," J. Phys.: Condens Matter, vol. 16, pp. R829-R858, June 2004.

[3] X. Zhou, S. Ge, D. Yao, Y. Zuo, Y. Xiao, "Effect of thermal treatment on room-temperature ferromagnetism in Co-doped ZnO powders," Physica B, vol. 403, pp. 3336-3339, September 2008.

[4] G. Hua, Y. Zhang, C. Ye, M. Wang and L. Zhang, "Controllable growth of ZnO nanoarrays in aqueous solution and their optical properties," Nanotechnology, vol. 18, pp. 145605(6pp), January 2007.

[5] J. H. He, J. H. Hsu, C. W. W. Wang, H. N. Lin, L. J. Chenand and Z. L. Wang, "Patern and feature designed growth of ZnO nanowire arrays for vertical devices," J. Phys. Chem. B, vol. 110, pp. 50-53, 2006.

[6] J. Elias, R. Tena-Zaera, G. Y. Wang, and C. Levy-Clement, "Conversion of ZnO nanowires into nanotubes with tailored dimentions," Chem. Mater., vol. 20, pp. 6633-6637, October 2008.

[7] S Singh, N. Rama and M. S. R. Rao, "Influence of d-d transition bands on electrical resistivity in Ni doped polycrystalline ZnO,". Appl. Phys. Letts., vol. 88, pp. 222111(3 pages), June 2006.

[8] M. R. A. Bhuiyan, M. K. Rahman, synthesis and characterization of Ni doped ZnO nanoparticles," Inter. J. Res., vol. 1, pp. 66-72, April 2014.

[9] K. Anbalagan, "UV-Sensitized Generation of Phase pure Cobalt-Doped Anatase:$Co_xTi_{1-x}O_{2-\delta}$ Nanocrystals with Ferromagnetic Behavior Using Nano-TiO_2/cis-$[Co^{III}(en)_2(MeNH_2)Cl]^{2+}$," J. Phys. Chem. C, vol. 115, pp. 3821-3832, February 2011.

[10] A. S. Ganeshraja and K. Anbalagan, "Synthesis and characterization of Co/nano-TiO_2 using Uv light irradiation of $Co^{II}(pic)_4Cl_2$ complex with nano-TiO_2," Int. J. Nanotech. Appl. vol. 6, pp. 127-131, 2012.

[11] A. S. Ganeshraja, K. Anbalagan, "participation of nanocrystalline TiO_2 surface in the electron transfer between semiconductor solid and adsorbed cobalt(III)-Rpy complex," Nano Systems: Phys. Chem. Math., vol. 4, pp. 276–287, 2013.

[12] S. Thirumurugan and K. Anbalagan, "Interfacial electron transfer reaction between $[Co^{III}(en)_2(Im)Cl]^{2+}$ complex ion and excited nano-ZnO surface," Int. J. Nanotech. Appl. vol. 6, pp. 248-252, 2012.

[13] N. Ashkenov, B. N. Mbenkum, C. Bundesmann, V. Riede, M. Lorenz, D. Spemann, E. M. Kaidashev, A. Kasic, M. Schubert, M. Grundmann, G. Wagner, H. Neumann, V. Darakchieva, H. Arwin, and B. Monemar, "Infrared dielectric functions and phonon modes of high-quality ZnO films," J. Appl. Phys. vol. 93, pp. 126-133, January 2003.

[14] M. Silambarasan, S. Saravanan, N. Ohtani and T. Soga, "Structural and optical studies of pure and Ni-doped ZnO nanoparticles synthesized by simple solution combustion method," Jpn. J. Appl. Phys. vol. 53, pp. 05FB16(1-7), April 2014.

[15] B. Cao, W. Cai, H. Zeng, and G. Duan, "Morphology evolution and photoluminescence properties of ZnO films electrochemically deposited on conductive glass substrates," J. Appl. Phys. vol. 99, 073516(6 pages), April 2006.

[16] S. Kumar, S. Mukherjee, R. K. Singh, S. Chatterjee, and A. K. Ghosh, "Structural and optical properties of sol-gel derived nanocrystalline Fe-doped ZnO," J. Appl. Phys. vol. 110, 103508(7 pages), November 2011.

[17] L. B. Duan, G. H. Rao, Y. C. Wang, J. Yu, and T. Wang, "Magnetization and Raman scattering studies of (Co,Mn) codoped ZnO nanoparticles," J. Appl. Phys. vol. 104, pp. 013909(5 pages), July 2008.

[18] S. Sakthivel, M.V. Shankar, M. Palanichamy, B. Arabindoo, D.W. Bahnemann, V. Murugesan, "Enhancement of photocatalytic activity by metal deposition: characterisation and photonic efficiency of Pt, Au and Pd deposited on TiO_2 catalyst," Water Research, vol. 38, pp. 3001-3008, July 2004.

[19] T. L. Tan, C. W. Lai, and S. B. A. Hamid, J. Nanomater., vol. 2014, Article ID 371720(pages 1-6), January 2014.